The importance of vibrational anharmonicity for electron-phonon coupling in molecular crystals

Antonios M. Alvertis[1, 2, *] and Edgar A. Engel[1, †]

[1] *Cavendish Laboratory, University of Cambridge,*
J. J. Thomson Avenue, Cambridge CB3 0HE, United Kingdom
[2] *Materials Sciences Division, Lawrence Berkeley National Laboratory, Berkeley, California 94720, USA*
(Dated: August 16, 2022)

Accurate predictions of electronic bandgaps are key to the computational design of functional materials with tailored optical and thermoelectric properties. While an accurate description of the underlying electronic structure is indispensable, electron-phonon interactions also play a prominent role in determining the bandgap. The harmonic vibrational approximation is used almost universally to describe electron-phonon coupling and provides a satisfactory description in most systems. Here we demonstrate that this is not the case for molecular crystals due to the presence of strongly anharmonic motions. We demonstrate the breakdown of the harmonic approximation in acene molecular crystals, and show that converged bandgaps can be obtained by rigorously accounting for vibrational anharmonicity using path-integral molecular dynamics. Finally, we characterise the most anharmonic vibrational modes and their contributions to the bandgap renormalisation.

Introduction.– Electronic bandgaps are a key quantity in studying the optical and electrical properties of materials and are central to applications such as photovoltaics [1] and thermoelectrics [2]. Accurate predictions of bandgaps are critical in understanding how the electronic and optical properties may be tuned by factors such as atomic or molecular substitutions, temperature [3–5], and pressure [6, 7], and thus for the design of materials with tailored characteristics. General predictive calculations of the electronic properties of materials require not only an accurate description of the electronic structure of a fixed atomic configuration, but also the rigorous treatment of quantum and thermal nuclear fluctuations, which can lead to a significant renormalisation and temperature dependence of bandgaps [8, 9].

Traditionally this electron-phonon coupling is either neglected, or accounted for subject to approximations [4]. In particular, nuclear motion is generally assumed to be harmonic, in which case the nuclear density distribution can be computed analytically and used to sample the ensemble average bandgap [4]. This approach has proven practical and suitable for a wide range of semiconductors [8–10]. Unfortunately, the harmonic vibrational approximation (HA) breaks down for general molecular systems. This is well-established in the context of computing thermodynamic stability [11–16], but more rarely discussed in the context of electron-phonon coupling and computational spectroscopy.

In this letter, we calculate fully anharmonic, quantum-mechanical, finite-temperature electronic bandgaps, and identify the phonons that most strongly deviate from the harmonic behaviour. This is achieved by employing path-integral molecular dynamics (PIMD) to sample the full anharmonic, quantum-mechanical thermodynamic ensemble and subsequently computing the associated bandgaps. To render these otherwise prohibitively expensive PIMD simulations feasible, we use a surrogate machine-learning (ML) potential, constructed to reproduce the potential energy surface from first-principles density functional theory (DFT) calculations. We restrict ourselves to DFT electronic bandgaps, reserving the extension to more sophisticated techniques for future work. While DFT using (semi-)local density functionals tends to severely underestimate bandgaps [17, 18], it provides the foundation for more accurate but computationally demanding techniques such as diffusion Monte Carlo [19] and *GW* many-body perturbation theory [20].

Using the example of the acene molecular crystals, we highlight the catastrophic failure of bandgap calculations based on the HA in the presence of anharmonic crystal vibrations, and identify which phonons dominate the electron-phonon interaction at different temperatures. Our approach could be utilised to rigorously compute the bandgaps of various materials where anharmonicity becomes important, such as lead-halide perovskites [21, 22].

Systems and methods.– To demonstrate the impact of nuclear vibrational anharmonicity on electron-phonon coupling in organic molecular crystals, we use the acene series, including naphthalene (Np), anthracene (Ac), tetracene (Tc), and pentacene (Pc). These systems consist of an increasing number of fused benzene rings (see Figure 1, top left panel). In every case we report the minimum bandgap of the studied systems. The electronic and optical properties of these acenes have been the topic of a previous study, which found evidence of strong effects of anharmonicity [23]. Details regarding the structures, geometry optimisations, *etc.* are provided in Supplemental Material [24] section II.A.

We compute first-principles ensemble-average bandgaps within the adiabatic approximation

$$E_g = \langle E_g(X) \rangle_{\mathcal{H}} = \frac{1}{Z} \int dX E_g(X) e^{-\beta V(X)} \quad (1)$$
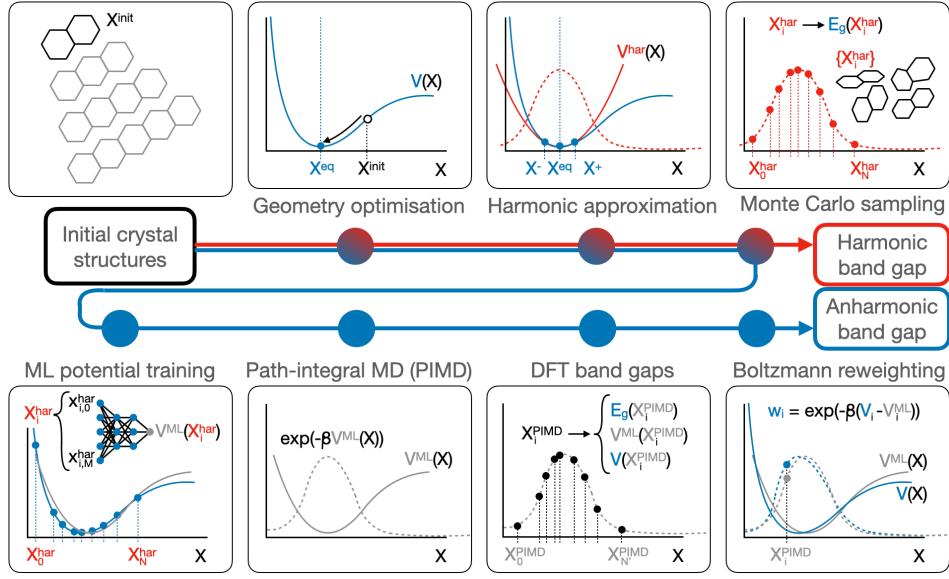
FIG. 1. Schematic of the key steps in obtaining first-principles bandgaps within the harmonic approximation, and upon rigorous sampling of anharmonic quantum nuclear fluctuations. For simplicity, we show a single (phonon) degree of freedom X. The approximate harmonic potential $V^{\text{har}}(X)$ (solid line), the corresponding Gaussian probability distribution (dashed line), and samples X^{har} drawn therefrom (filled circles) are highlighted in red, while the approximate surrogate ML potential $V^{\text{ML}}(X)$ and associated probability distribution and samples are shown in grey, and the rigorous, first-principles potential $V(X)$, distribution and Boltzmann weights are indicated in blue. The crystal structures are represented in terms of their molecular building blocks.

where the canonical partition function $Z = \int dX e^{-\beta V(X)}$ involves the configuration space integral $\int dX$ [25]. We pursue a three-pronged approach. We first geometry optimise the different acenes (Fig. 1, panel 2), and extract the respective "static" bandgaps, E_g^{st}, which provide the reference for computing vibrational bandgap corrections.

Second, we compute the bandgap within the HA, which amounts to approximating the physical Hamiltonian $\mathcal{H}$ with

$$\mathcal{H}^{\text{har}} \equiv \frac{1}{2} \sum_{n,\mathbf{q}} \nabla^2_{u_{n,\mathbf{q}}} + V^{\text{har}}; \quad V^{\text{har}} \equiv \frac{1}{2} \sum_{n,\mathbf{q}} \omega^2_{n,\mathbf{q}} u^2_{n,\mathbf{q}} \tag{2}$$

(in atomic units). This primarily serves the purpose of providing atomistic insight by resolving the phonons, labelled by branch index n and wavevector $\mathbf{q}$, and (subsequently) their respective contributions to the vibrational bandgap correction. We compute the ensemble-average E_g^{har} using a finite-displacements approach [26, 27] to compute phonon frequencies $\{\omega_{n,\mathbf{q}}\}$ and coordinates $\{u_{n,\mathbf{q}}\}$ (panel 3), and then draw N random samples $\{X_i^{\text{har}}\}$ from the multivariate Gaussian phonon distribution and calculate their bandgaps $\{E_g(X_i^{\text{har}})\}$ (panel 4). E_g^{har} is then simply computed as the average bandgap of the samples

$$E_g^{\text{har}} = \lim_{N \to \infty} \frac{1}{N} \sum_{i=1}^{N} E_g(X_i^{\text{har}}) \tag{3}$$

This provides a non-perturbative description of electron-

phonon coupling [8], *within the constraints of the approximate harmonic vibrational distribution*. Unfortunately, the systematic error resulting from the HA cannot be quantified reliably.

To rigorously account for general, anharmonic quantum nuclear motion we finally employ path-integral techniques. Since converged first-principles PIMD simulations for our structures are prohibitively expensive, we use the total energies and forces computed as a side product of sampling E_g^{har} to train a surrogate ML potential, V^{ML} (grey solid, Fig. 1, panel 5). We chose the tried-and-tested Behler-Parinello framework as implemented in the N2P2 package [28], in which structures are encoded in atom-centred symmetry functions [29] and passed through fully-connected feed-forward artificial neural networks to compute atomic forces and contributions to the total energy. We replicate the architecture, which has previously proven highly accurate and reliable for polymorphs of benzene [30, 31]. In result, the evaluation of V^{ML} is orders of magnitude less expensive than a corresponding first-principles calculation, which renders PIMD simulations using the ML Hamiltonian,

$$\mathcal{H}^{\text{ML}} \equiv \sum_{i=1}^{N_a} \frac{\hat{\mathbf{p}}_i^2}{2m_i} + V^{\text{ML}}(\hat{\mathbf{r}}_1, \dots, \hat{\mathbf{r}}_{N_a}) \tag{4}$$

computationally tractable. This permits us to compute the bandgap of the ML ensemble as the average over the DFT values computed for a small number N', of sample

structures $\{X_i^{\mathrm{ML}}\}$ drawn from a PIMD trajectory:

$$E_g^{\mathrm{ML}} = \lim_{N'\to\infty} \frac{1}{N'} \sum_{i=1}^{N'} E_g(X_i^{\mathrm{ML}}). \qquad (5)$$

In practice we find that computing the DFT bandgap for between 50 (for the larger supercells) and 200 (for the unit cells) configurations from PIMD trajectories for 32 beads at regular intervals of 50 fs, provides suitably converged ensemble average bandgaps.

Crucially, the affordability of V^{ML} comes at the price of residual errors with respect to the reference V, which may arise from the short-ranged nature of the ML potential [32], information lost during the "featurisation" of the samples [33], or from limited data. While the root-mean-squared (RMS) errors in ML energies and forces do not exceed 3.1 meV/atom and 0.16 eV/Angstrom, except for naphthalene, they stand to affect the bandgap estimates. To quantify this we use the first-principles potentials $\{V(X_i^{\mathrm{ML}})\}$, which come as a complement of evaluating the corresponding bandgaps (Eq. 5), to extract the first-principles bandgap E_g by statistical reweighting of the samples obtained from the ML ensemble (panel 8):

$$E_g = \lim_{N'\to\infty} \frac{\sum_{i=1}^{N'} w(X_i^{\mathrm{ML}}) E_g(X_i^{\mathrm{ML}})}{\sum_{i=1}^{N'} w(X_i^{\mathrm{ML}})} \qquad (6)$$
$$w_i \equiv \exp\left(-\beta\left(V(X_i^{\mathrm{ML}}) - V^{\mathrm{ML}}(X_i^{\mathrm{ML}})\right)\right)$$

Recovering the DFT bandgaps E_g for the unit cells of acenes using equation (6) reveals a consistent overestimation of the bandgap correction for all acenes using V^{ML}, which does not affect the trends and microscopic insights discussed below. This overestimation is largest for naphthalene (97 meV) and much smaller for the larger acenes, consistent with smaller errors in V^{ML} for these systems.

For the acenes, applying the same reweighting strategy to recover E_g from the sampled $\{E_g(X_i^{\mathrm{har}})\}$ is prevented by substantial differences between $V^{\mathrm{har}}(X)$ and $V(X)$, leading to diverging weights and unphysical bandgap estimates, which do not agree with those obtained using PIMD. However, since statistical reweighting can be attempted at no additional cost in terms of DFT calculations, for near-harmonic systems it provides a practical means of probing for anharmonic effects and avoiding unnecessary PI calculations.

Results.– Let us demonstrate the breakdown of the HA in the case of anthracene at $T = 300$ K. As visualised in Figure 2a, the harmonic correction to the static bandgap (red) fails to converge with increasing supercell size. Meanwhile, accounting for anharmonic effects leads to smooth convergence up to large, size 27 $(3 \times 3 \times 3)$ supercells. To elucidate the disagreement between the two cases, we project the harmonic and anharmonic trajectories of anthracene onto the phonon coordinates $\{u_{n,\mathbf{q}}\}$. This allows us to compare the RMS displacement $\sqrt{\langle u_{n,\mathbf{q}}^2 \rangle}$ of each phonon mode $(n,\mathbf{q})$ at the two levels

of theory. Figure 2b shows significant differences in the RMS displacements of low-frequency phonons, and highlights two particularly anharmonic modes (black circle and arrow) that involve sliding motions between several anthracene molecules as shown in the inset. In Figure 2c we plot the harmonic potential energy surface along the phonon coordinate $u_{n,\mathbf{q}}$ of one of the two modes and compare it to the true, fully-anharmonic potential along $u_{n,\mathbf{q}}$ as obtained through direct DFT calculations. We see that the true potential is much stiffer than its HA and, in comparison, stifles the amplitude of the vibrational motion. This is consistent with the corresponding harmonic and anharmonic RMS displacements observed in Figure 2b, and suggests that the HA leads to unphysically large phonon amplitudes, which in turn result in the lack of convergence for the harmonic bandgap seen in Figure 2a.

The breakdown of the HA is not limited to the case of anthracene. In Supplemental Material [24] Section III, we show that the remaining acenes exhibit similar behaviour, with strongly anharmonic low-frequency phonons, which can in turn manifest a similar lack of convergence for the harmonic bandgap. Such anharmonicity generally arises when studying supercells of size four or above, where phonons can primarily involve intermolecular motion between several molecules, resulting in extremely low-frequency anharmonic motion, particularly for (but not limited to) acoustic modes. Consequently, studies using coarse $\mathbf{q}$-grids (or, conversely, small simulation cells within finite-displacement approaches) may escape the breakdown of the HA and obtain reasonable estimates of vibrationally-renormalised bandgaps of molecular crystals [23]. However, this generally comes at the price of errors due to unconverged $\mathbf{q}$-sampling (in particular, neglecting low-frequency $\mathbf{q} \to 0$ phonons), as apparent in Figures 2a and 3a. Accurate bandgap predictions thus require studying large supercells, which exhibit strong anharmonicity. Notably, the degree of anharmonicity is fairly insensitive to the flavour of electronic structure theory, as shown for of pentacene in Supplemental Material [24] Section III.

Therefore, in order to rigorously account for electron-phonon interactions in molecular crystals, we turn to the aforementioned PIMD approach, which fully accounts for anharmonicity and nuclear quantum effects. Figure 3a shows that the room-temperature bandgap renormalisation of the acene crystals converges smoothly with increasing supercell size. Pentacene and tetracene bandgaps are already reasonably well-converged for supercells of size two. The bandgaps only show marginal changes when increasing the supercell size to eight, which is the maximum we were able to simulate for these systems, due to memory limitations in the DFT bandgap calculations for the sampled configurations. For the smaller acenes, larger supercells are required to reach convergence and even for the $3 \times 3 \times 3$ case naphthalene and anthracene seem to not be fully converged. However, DFT calculations on larger supercells are prohibitively
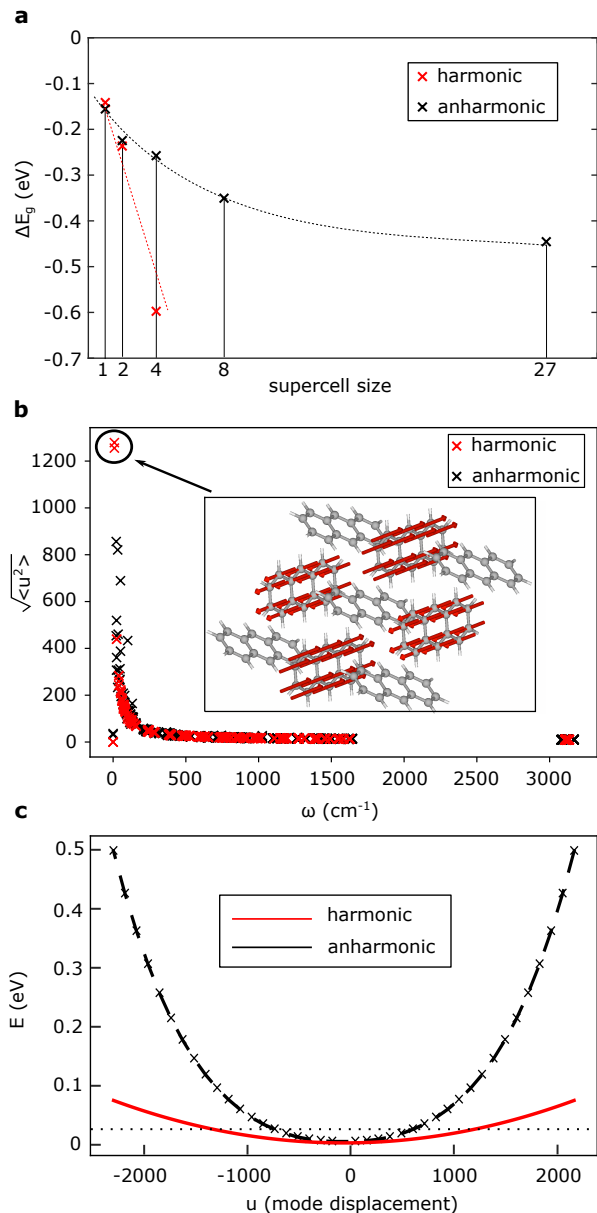
FIG. 2. Harmonic and anharmonic bandgap renormalisation in anthracene at 300 K (panel **a**). The root-mean-squared phonon displacements in the two distributions (panel **b**) highlight unphysical displacements for harmonic low-frequency phonons. For one of these motions, the harmonic and anharmonic potential energy surface is shown in panel **c**, where room temperature is marked with a dotted line. This phonon involves a sliding motion between several molecules (panel **d**).

expensive. More details regarding the convergence of PIMD averages are given in SI [24] Section II.

Comparing our value of $-0.683\,\text{eV}$ for the room-temperature bandgap renormalisation in naphthalene to the $-0.44\,\text{eV}$ [34] obtained using density functional perturbation theory (DFPT) [35, 36] and Allen-Heine-Cardona (AHC) theory highlights the differences arising from different approximations to the electron-phonon
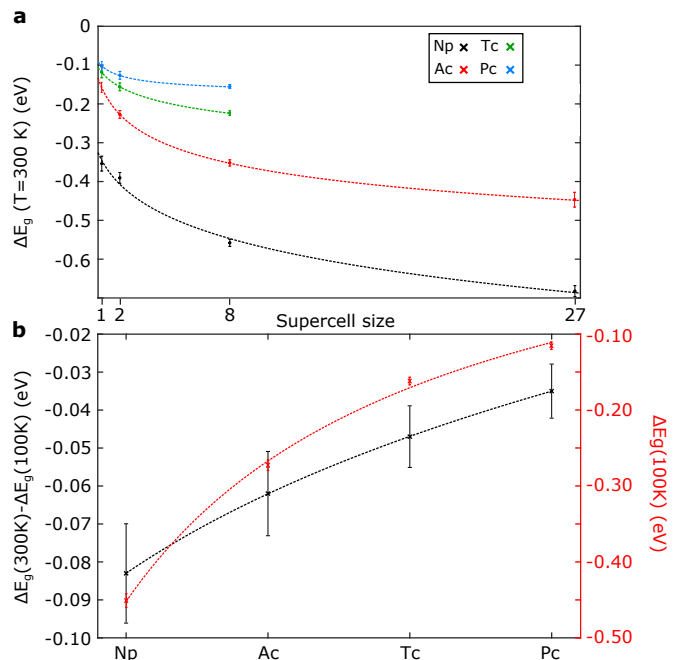

FIG. 3. Bandgap renormalisation of the acene crystals, computed with path integral molecular dynamics. Convergence of the bandgap correction at 300 K with respect to the simulation cell size (panel **a**). Panel **b** shows the difference between the converged 100 K and 300 K corrections (black), as well as the bandgap renormalisation at 100 K (red).

interaction. While Ref. [34] relies on the HA and perturbation theory, our PIMD approach naturally includes anharmonicity and higher-order terms in the electron-phonon interaction. The latter are known to be important in molecular crystals [8] and are reflected, for instance, in the non-quadratic dependence of pentacene bandgap on the displacement of low-frequency phonons shown in Supplemental Material [24] Figure 4b. We also note that the lack of convergence of the bandgap that we observe within the HA is not related to the divergence which can appear in AHC theory, particularly for IR-active materials [37], where it can be remedied by including non-adiabatic effects. We expect our results for the acene crystals (unlike more ionic materials [38]) to be insensitive to non-adiabatic effects. Moreover, we emphasise that the unphysical effects that arise from neglecting the effects of anharmonicity on electron-phonon coupling are not an artefact of finite displacement methods, as similar observations have been reported for $SrTiO_3$ within AHC theory [39].

Figure 3a highlights larger bandgap corrections for smaller molecular crystals. It is however not yet clear whether the differences in the bandgap renormalisation of the acenes are due to thermal or quantum nuclear motion. To answer this question, we also sample the bandgaps at 100 K using PIMD. In Figure 3b, we plot the difference between the bandgaps at 100 K and 300 K (black). This purely temperature-driven renormalisa-

tion is more pronounced for smaller acenes, indicating that thermally-activated low-frequency phonons are more strongly coupled to the bandgaps of these systems. The remaining bandgap renormalisation at $100\,\mathrm{K}$ (red) is also stronger for the smaller systems. At low temperatures nuclear quantum fluctuations due to high-frequency phonons dominate, since thermal activation is minimal, while these modes have significant zero-point energies $\hbar\omega_{n,\mathbf{q}}/2$. To further elucidate the different coupling of low- and high-frequency phonons to the acene bandgaps, we compute the phonon-resolved bandgap renormalisation within a quadratic approximation, which confirms the above picture (see Supplemental Material [24] Section IV).

Finally, it is interesting to visualise the phonons which most strongly couple to electrons as a result of thermal activation (see Supplemental Material [24] Section V). Rotations around the molecular long-axes lead to significant bandgap renormalisation in all studied systems, and increasingly so for the smaller acenes. Naphthalene is the only system with significant contributions from rotations around the molecular short-axis, which drive the failure of the harmonic approximation. We hypothesise that such short-axis rotations become energetically unfavourable for larger acenes, increasing the frequency of these phonons beyond the threshold of thermal activation at room temperature. Highly anharmonic sliding motions (such as the one in Figure 2b) become important in the larger acenes and result in a *blue-shift* of the gap (see Supplemental Material [24] Section III). The anharmonic character of these motions, as well as their importance for phenomena such as charge transport and singlet fission in organic crystals are well known [40–42].

Conclusions.– In this letter we have demonstrated the breakdown of the HA for computing electron-phonon effects and associated thermodynamic averages of observables for molecular crystals. We have presented an integrated approach for rigorously including anharmonic effects in calculations of electron-phonon coupling within the adiabatic approximation, showing that it permits computing converged values for the phonon-induced bandgap renormalisation of the acene crystals. We find that both low- and high-frequency vibrations couple more strongly to the bandgap of crystals consisting of smaller molecules, which we discuss in light of the displacement patterns of specific phonon modes. Sliding motions are consistently found to be amongst the most anharmonic ones, emphasising the need to rigorously include anharmonicity in the study of phenomena such as charge transport and singlet fission where these are known to be important.

In the acenes the breakdown of the HA is driven by low-frequency, acoustic phonons, which are only probed for fine sampling of the Brillouin zone. However, vibrational anharmonicity is a recurrent theme in functional materials and more generally plays prominent roles in determining material properties, such as in the dynamic stabilisation of halide perovskites [43] and the cubic perovskite phase of $SrTiO_3$ [14]. We thus emphasise that our approach for capturing anharmonic effects is universal (albeit subject to the adiabatic approximation) and applicable to diverse materials. Given the demonstrable importance of non-adiabatic effects for electron-phonon coupling in more ionic materials [38], it will be interesting to investigate the interplay of non-adiabaticity and vibrational anharmonicity.

[1] M. A. Green, Photovoltaic technology and visions for the future, Progress in Energy **1**, 013001 (2019).

[2] J. Sofo and G. D. Mahan, Optimum band gap of a thermoelectric material, Physical Review B **49**, 4565 (1994).

[3] P. B. Allen and V. Heine, Theory of the temperature dependence of electronic band structures, Journal of Physics C: Solid State Physics **9**, 2305 (1976).

[4] S. Poncé, G. Antonius, Y. Gillet, P. Boulanger, J. Laflamme Janssen, A. Marini, M. Côté, and X. Gonze, Temperature dependence of electronic eigenenergies in the adiabatic harmonic approximation, Physical Review B - Condensed Matter and Materials Physics **90**, 10.1103/PhysRevB.90.214304 (2014), 1408.2752.

[5] W. A. Saidi, S. Poncé, and B. Monserrat, Temperature Dependence of the Energy Levels of Methylammonium Lead Iodide Perovskite from First-Principles, Journal of Physical Chemistry Letters **7**, 5247 (2016), 1612.01530.

[6] S. K. Yadav, T. Sadowski, and R. Ramprasad, Density functional theory study of ZnX (X=O, S, Se, Te) under uniaxial strain, Physical Review B - Condensed Matter and Materials Physics **81**, 1 (2010).

[7] V. Gorelov, M. Holzmann, D. M. Ceperley, and C. Pierleoni, Energy Gap Closure of Crystalline Molecular Hydrogen with Pressure, Physical Review Letters **124**, 116401 (2020), 1911.06135.

[8] B. Monserrat, E. A. Engel, and R. J. Needs, Giant electron-phonon interactions in molecular crystals and the importance of nonquadratic coupling, Physical Review B - Condensed Matter and Materials Physics **92**, 1 (2015).

[9] G. Antonius, S. Poncé, P. Boulanger, M. Côté, and X. Gonze, Many-body effects on the zero-point renormal-

[9] ization of the band structure, Physical Review Letters **112**, 1 (2014).

[10] P. Han and G. Bester, Large nuclear zero-point motion effect in semiconductor nanoclusters, Physical Review B **88**, 165311 (2013).

[11] O. Hellman, I. A. Abrikosov, and S. I. Simak, Lattice dynamics of anharmonic solids from first principles, Physical Review B **84**, 180301(R) (2011).

[12] B. Monserrat, N. D. Drummond, and R. J. Needs, Anharmonic vibrational properties in periodic systems: energy, electron-phonon coupling, and stress, Physical Review B **87**, 144302 (2013).

[13] I. Errea, M. Calandra, and F. Mauri, Anharmonic free energies and phonon dispersions from the stochastic self-consistent harmonic approximation: Application to platinum and palladium hydrides, Physical Review B **89**, 064302 (2014).

[14] T. Tadano and S. Tsuneyuki, Self-consistent phonon calculations of lattice dynamical properties in cubic SrTiO3 with first-principles anharmonic force constants, Physical Review B **92**, 054301 (2015).

[15] S. E. Brown and V. A. Mandelshtam, Self-consistent phonons: An accurate and practical method to account for anharmonic effects in equilibrium properties of general classical or quantum many-body systems, Chemical Physics **481**, 69 (2016).

[16] V. Kapil, E. A. Engel, M. Rossi, and M. Ceriotti, Assessment of Approximate Methods for Anharmonic Free Energies, J. Chem. Theory Comput. **15**, 5845 (2019).

[17] R. W. Godby, M. Schlüter, and L. J. Sham, Accurate Exchange-Correlation Potential for Silicon and Its Discontinuity on Addition of an Electron, Physical Review Letters **56**, 2415 (1986).

[18] R. W. Godby, M. Schlüter, and L. J. Sham, Self-energy operators and exchange-correlation potentials in semiconductors, Physical Review B **37**, 10159 (1988).

[19] R. J. Needs, M. D. Towler, N. D. Drummond, and P. López Ríos, Continuum variational and diffusion quantum Monte Carlo calculations, Journal of Physics Condensed Matter **22**, 10.1088/0953-8984/22/2/023201 (2010), 1002.2127.

[20] M. S. Hybertsen and S. G. Louie, Electron correlation in semiconductors and insulators: Band gaps and quasiparticle energies, Physical Review B **34**, 5390 (1986).

[21] C. Gehrmann and D. A. Egger, Dynamic shortening of disorder potentials in anharmonic halide perovskites, Nature Communications **10**, 10.1038/s41467-019-11087-y (2019).

[22] M. Sendner, P. K. Nayak, D. A. Egger, S. Beck, C. Müller, B. Epding, W. Kowalsky, L. Kronik, H. J. Snaith, A. Pucci, and R. Lovrinčić, Optical phonons in methylammonium lead halide perovskites and implications for charge transport, Materials Horizons **3**, 613 (2016), 1607.08541.

[23] A. M. Alvertis, R. Pandya, L. A. Muscarella, N. Sawhney, M. Nguyen, B. Ehrler, A. Rao, R. H. Friend, A. W. Chin, and B. Monserrat, Impact of exciton delocalization on exciton-vibration interactions in organic semiconductors, Phys. Rev. B **102**, 081122 (2020).

[24] See supplemental material at [url will be inserted by the production group] which includes references [44–66] for computational details, an extensive discussion of methods for bandgap calculations, and a (mode-resolved) picture of anharmonicity in acene crystals.

[25] C. E. Patrick and F. Giustino, Unified theory of electron–phonon renormalization and phonon-assisted optical absorption, Journal of Physics: Condensed Matter **26**, 365503 (2014).

[26] G. Kresse, J. Furthmüller, and J. Hafner, Ab initio Force Constant Approach to Phonon Dispersion Relations of Diamond and Graphite, Europhysics Letters **32**, 729 (1995).

[27] K. Parlinski, Z. Q. Li, and Y. Kawazoe, First-Principles Determination of the Soft Mode in Cubic ZrO_2, Physical Review Letters **78**, 4063 (1997).

[28] A. Singraber, N2P2, https://github.com/CompPhysVienna/n2p2.

[29] J. Behler and M. Parrinello, Generalized Neural-Network Representation of High-Dimensional Potential-Energy Surfaces, Phys. Rev. Lett. **98**, 146401 (2007).

[30] E. A. Engel, V. Kapil, and M. Ceriotti, Importance of nuclear quantum effects for nmr crystallography, J. Phys. Chem. Lett. **12**, 7701 (2021).

[31] V. Kapil and E. A. Engel, A complete description of thermodynamic stabilities of molecular crystals, Proc. Natl. Acad. Sci. U.S.A. **119**, e2111769119 (2022).

[32] A. Grisafi and M. Ceriotti, Incorporating long-range physics in atomic-scale machine learning, J. Chem. Phys. **151**, 204105 (2019).

[33] S. N. Pozdnyakov, M. J. Willatt, A. P. Bartók, C. Ortner, G. Csányi, and M. Ceriotti, Incompleteness of Atomic Structure Representations, Phys. Rev. Lett. **125**, 166001 (2020).

[34] F. Brown-Altvater, G. Antonius, T. Rangel, M. Giantomassi, C. Draxl, X. Gonze, S. G. Louie, and J. B. Neaton, Band gap renormalization, carrier mobilities, and the electron-phonon self-energy in crystalline naphthalene, Physical Review B **101**, 1 (2020).

[35] S. Baroni, S. De Gironcoli, A. Dal Corso, and P. Giannozzi, Phonons and related crystal properties from density-functional perturbation theory, Reviews of Modern Physics **73**, 515 (2001), arXiv:9702376 [hep-ph].

[36] C. Verdi and F. Giustino, Fröhlich electron-phonon vertex from first principles, Physical Review Letters **115**, 1 (2015), 1510.06373.

[37] S. Poncé, Y. Gillet, J. Laflamme Janssen, A. Marini, M. Verstraete, and X. Gonze, Temperature dependence of the electronic structure of semiconductors and insulators, Journal of Chemical Physics **143**, 10.1063/1.4927081 (2015), 1504.05992.

[38] A. Miglio, V. Brousseau-Couture, E. Godbout, G. Antonius, Y. H. Chan, S. G. Louie, M. Côté, M. Giantomassi, and X. Gonze, Predominance of non-adiabatic effects in zero-point renormalization of the electronic band gap, npj Computational Materials **6**, 10.1038/s41524-020-00434-z (2020), 2011.12765.

[39] Y. N. Wu, W. A. Saidi, J. K. Wuenschell, T. Tadano, P. Ohodnicki, B. Chorpening, and Y. Duan, Anharmonicity Explains Temperature Renormalization Effects of the Band Gap in SrTiO3, Journal of Physical Chemistry Letters **11**, 2518 (2020).

[40] A. Troisi, G. Orlandi, and J. E. Anthony, Electronic interactions and thermal disorder in molecular crystals containing cofacial pentacene units, Chemistry of Materials **17**, 5024 (2005).

[41] G. Schweicher, G. D'Avino, M. T. Ruggiero, D. J. Harkin, K. Broch, D. Venkateshvaran, G. Liu, A. Richard, C. Ruzié, J. Armstrong, A. R. Kennedy,

K. Shankland, K. Takimiya, Y. H. Geerts, J. A. Zeitler, S. Fratini, and H. Sirringhaus, Chasing the "Killer" Phonon Mode for the Rational Design of Low-Disorder, High-Mobility Molecular Semiconductors, Advanced Materials **31**, 10.1002/adma.201902407 (2019).

[42] H. Seiler, M. Krynski, D. Zahn, S. Hammer, Y. W. Windsor, T. Vasileiadis, J. Pflaum, R. Ernstorfer, M. Rossi, and H. Schwoerer, Nuclear dynamics of singlet exciton fission: a direct observation in pentacene single crystals, Science Advances **7**, eabg0869 (2021).

[43] J. S. Bechtel, J. C. Thomas, and A. Van Der Ven, Finite-temperature simulation of anharmonicity and octahedral tilting transitions in halide perovskites, Physical Review Materials **3**, 1 (2019).

[44] J. M. Robertson, V. C. Sinclair, and J. Trotter, The crystal and molecular structure of tetracene, Acta Crystallographica **14**, 697 (1961).

[45] M. J. Willatt, F. Musil, and M. Ceriotti, Feature optimization for atomistic machine learning yields a data-driven construction of the periodic table of the elements, Phys Chem Chem Phys **20**, 29661 (2018).

[46] V. Kapil, M. Rossi, O. Marsalek, R. Petraglia, Y. Litman, T. Spura, B. Cheng, A. Cuzzocrea, R. H. Meißner, D. M.Wilkins, B. A. Helfrecht, P. Juda, S. P. Bienvenue, W. Fang, J. Kessler, I. Poltavsky, S. Vandenbrande, J. Wieme, and M. Ceriotti, i-PI 2.0: A universal force engine for advanced molecular simulations, Computer Physics Communications **236**, 214 (2018).

[47] Y. Eldar, M. Lindenbaum, M. Porat, and Y. Y. Zeevi, The Farthest Point Strategy for Progressive Image Sampling, IEEE Transactions on Image Processing **6**, 1305 (1997).

[48] V. Kapil, J. Behler, and M. Ceriotti, High order path integrals made easy, The Journal of Chemical Physics **145**, 234103 (2016).

[49] G. Imbalzano, A. Anelli, D. Giofré, S. Klees, J. Behler, and M. Ceriotti, Automatic selection of atomic fingerprints and reference configurations for machine-learning potentials, J. Chem. Phys. **148**, 241730 (2018).

[50] B. Hourahine, B. Aradi, V. Blum, F. Bonafé, A. Buccheri, C. Camacho, C. Cevallos, M. Y. Deshaye, T. Dumitrică, A. Dominguez, S. Ehlert, M. Elstner, T. van der Heide, J. Hermann, S. Irle, J. J. Kranz, C. Köhler, T. Kowalczyk, T. Kubař, I. S. Lee, V. Lutsker, R. J. Maurer, S. K. Min, I. Mitchell, C. Negre, T. A. Niehaus, A. M. N. Niklasson, A. J. Page, A. Pecchia, G. Penazzi, M. P. Persson, J. Řezáč, C. G. Sánchez, M. Sternberg, M. Stöhr, F. Stuckenberg, A. Tkatchenko, V. W.-z. Yu, and T. Frauenheim, Dftb+, a software package for efficient approximate density functional theory based atomistic simulations, The Journal of Chemical Physics **152**, 124101 (2020).

[51] F. Musil, M. J. Willatt, M. A. Langovoy, and M. Ceriotti, Fast and Accurate Uncertainty Estimation in Chemical Machine Learning, J. Chem. Theory Comput. **15**, 906 (2019).

[52] M. Gaus, A. Goez, and M. Elstner, Parametrization and benchmark of dftb3 for organic molecules, Journal of Chemical Theory and Computation **9**, 338 (2013).

[53] S. C. Capelli, A. Albinati, S. A. Mason, and B. T. M. Willis, Molecular motion in crystalline naphthalene: Analysis of multi-temperature X-ray and neutron diffraction data, Journal of Physical Chemistry A **110**, 11695 (2006).

[54] P. Giannozzi, S. Baroni, N. Bonini, M. Calandra, R. Car, C. Cavazzoni, D. Ceresoli, G. L. Chiarotti, M. Cococcioni, I. Dabo, A. Dal Corso, S. Fabris, G. Fratesi, S. de Gironcoli, R. Gebauer, U. Gerstmann, C. Gougoussis, A. Kokalj, M. Lazzeri, L. Martin-Samos, N. Marzari, F. Mauri, R. Mazzarello, S. Paolini, A. Pasquarello, L. Paulatto, C. Sbraccia, S. Scandolo, G. Sclauzero, A. P. Seitsonen, A. Smogunov, P. Umari, and R. M. Wentzcovitch, QUANTUM ESPRESSO: a modular and open-source software project for quantum simulations of materials, Journal of Physics: Condensed Matter **21**, 395502 (2009).

[55] M. A. Morales, J. M. McMahon, C. Pierleoni, and D. M. Ceperley, Towards a predictive first-principles description of solid molecular hydrogen with density functional theory, Phys. Rev. B **87**, 184107 (2013).

[56] A. P. Bartók, R. Kondor, and G. Csányi, On representing chemical environments, Phys. Rev. B **87**, 184115 (2013).

[57] A. Tkatchenko and M. Scheffler, Accurate molecular van der Waals interactions from ground-state electron density and free-atom reference data, Physical Review Letters **102**, 6 (2009).

[58] M. Rossi, P. Gasparotto, and M. Ceriotti, Anharmonic and Quantum Fluctuations in Molecular Crystals: A First-Principles Study of the Stability of Paracetamol, Phys. Rev. Lett. **117**, 115702 (2016).

[59] J. P. Perdew, K. Burke, and M. Ernzerhof, Generalized Gradient Approximation Made Simple, Physical Review Letters **77**, 3865 (1996).

[60] M. Ceriotti, M. Parrinello, T. E. Markland, and D. E. Manolopoulos, Efficient stochastic thermostatting of path integral molecular dynamics, J. Chem. Phys. **133**, 124104 (2010).

[61] M. Gaus, X. Lu, M. Elstner, and Q. Cui, Parameterization of dftb3/3ob for sulfur and phosphorus for chemical and biological applications, Journal of Chemical Theory and Computation **10**, 1518 (2014).

[62] Y. Tajima, T. Matsuo, and H. Suga, Phase transition in KOH-doped hexagonal ice, Nature **299**, 810 (1982).

[63] H. J. Monkhorst and J. D. Pack, Special points for Brillouin-zone integrations, Physical Review B **13**, 5188 (1976).

[64] S. Haas, B. Batlogg, C. Besnard, M. Schiltz, C. Kloc, and T. Siegrist, Large uniaxial negative thermal expansion in pentacene due to steric hindrance, Physical Review B: Condensed Matter and Materials Physics **76**, 1 (2007).

[65] G. Imbalzano and M. Ceriotti, Modeling the ga/as binary system across temperatures and compositions from first principles, Phys. Rev. Mater. **5**, 063804 (2021).

[66] B. Cheng, E. A. Engel, J. Behler, C. Dellago, and M. Ceriotti, Ab initio thermodynamics of liquid and solid water, Proc. Natl. Acad. Sci. U.S.A. **116**, 1110 (2019).